

Type I interferon signaling deficiency results in dysregulated innate immune responses to SARS-CoV-2 in a mouse model

Journal:	<i>European Journal of Immunology - 2</i>
Manuscript ID	eji.202249913.R2
Wiley - Manuscript type:	Rapid Short Communication
Date Submitted by the Author:	12-Sep-2022
Complete List of Authors:	Ogger, Patricia; Imperial College London, NHLI/ Respiratory Infections Garcia Martin, Minerva; Imperial College London, NHLI/ Respiratory Infections Michalaki, Christina; Imperial College London, NHLI/ Respiratory Infections Zhou, Jie; Imperial College London, Department of Infectious Disease Brown, Jonathan; Imperial College London, Dept of Infectious Disease Du, Yue; University of Oxford, Radcliffe Department of Medicine Miah, Kamran; University of Oxford, Radcliffe Dept of Medicine Habib, Omar; University of Oxford, Radcliffe Dept of Medicine Hyde, Stephen; University of Oxford, Radcliffe Dept of Medicine Gills, Deborah; University of Oxford, Radcliffe Dept of Medicine Barclay, Wendy; Imperial College London, Dept of Infectious Disease Johansson, Cecilia; Imperial College London, NHLI/ Respiratory Infections
Keywords:	innate immune response, interferons, in vivo, monocytes, SARS-CoV-2
Keywords:	

SCHOLARONE™
Manuscripts

1
2
3
4 1 **Type I interferon signaling deficiency results in dysregulated innate immune**
5
6 2 **responses to SARS-CoV-2 in mice**
7
8 3

9 4 **Authors:** Patricia P. Ogger¹, Minerva Garcia Martín¹, Christina Michalaki¹, Jie Zhou², Jonathan C.
10 5 Brown², Yue Du³, Kamran M. Miah³, Omar Habib³, Stephen C. Hyde³, Deborah R. Gill³, Wendy S.
11 6 Barclay², Cecilia Johansson¹
12
13 7

14
15
16 8 ¹Section of Respiratory Infections, National Heart and Lung Institute, Imperial College London, St
17 9 Mary's Campus, W2 1PG

18
19 10 ²Department of Infectious Disease, Imperial College London, St Mary's Campus, W2 1PG

20 11 ³Radcliffe Department of Medicine (NDCLS), University of Oxford, OX3 9DU
21 12

22
23
24 13 Lead contact: Dr Cecilia Johansson, c.johansson@imperial.ac.uk
25

26 14 St Mary's Campus, National Heart and Lung Institute, Imperial College London, W2 1PG, UK.
27
28
29
30
31
32
33
34
35
36
37
38
39
40
41
42
43
44
45
46
47
48
49
50
51
52
53
54
55
56
57
58
59
60

Abstract:

SARS-CoV-2 is a newly emerged coronavirus, causing the global pandemic of respiratory coronavirus disease (COVID-19). The type I interferon (IFN) pathway is of particular importance for anti-viral defence and recent studies identified that type I IFNs drive early inflammatory responses to SARS-CoV-2. Here, we use a mouse model of SARS-CoV-2 infection, facilitating viral entry by intranasal recombinant Adeno-Associated Virus (rAAV) transduction of *hACE2* in wildtype (WT) and type I IFN-signalling-deficient (*Ifnar1*^{-/-}) mice, to study type I IFN signalling deficiency and innate immune responses during SARS-CoV-2 infection. Our data show that type I IFN signaling is essential for inducing anti-viral effector responses to SARS-CoV-2, control of virus replication and to prevent enhanced disease. Furthermore, *hACE2-Ifnar1*^{-/-} mice had increased gene expression of the chemokine *Cxcl1* and airway infiltration of neutrophils as well as a reduced and delayed production of monocyte-recruiting chemokine CCL2. *hACE2-Ifnar1*^{-/-} mice showed altered recruitment of inflammatory myeloid cells to the lung upon SARS-CoV-2 infection, with a shift from Ly6C⁺ to Ly6C⁻ expressing cells. Together, our findings suggest that type I IFN deficiency results in a dysregulated innate immune response to SARS-CoV-2 infection.

Keywords:

Innate Immune Response/ type I IFN / In vivo / SARS-CoV-2/ myeloid cells

69

70 Introduction

71 The ongoing coronavirus disease (COVID-19) pandemic caused by severe acute respiratory syndrome-
72 coronavirus 2 (SARS-CoV-2) has resulted in over 400 million cases in the first two years of the
73 pandemic. The estimated fatality rate lies between 1-2%, however this is considerably higher for
74 elderly patients over 80 years of age (~10%) and nursing home residents (>20%) (1). Type I interferons
75 (IFNs) are one of the first responses elicited against viral infection and they induce anti-viral defense
76 mechanisms by binding to the IFN- α/β receptor (IFNAR) and signaling through the JAK-STAT pathway.
77 This induces expression of IFN stimulated genes (ISG), resulting in expression of anti-viral effector
78 proteins that restrict viral replication and activation of immune cells via induction of chemokine and
79 cytokine production (2), including CXCL10 and CCL2 (3). Early *in vitro* studies using human bronchial
80 epithelial cell lines infected with SARS-CoV-2 showed decreased production of type I and III IFNs
81 coupled with low anti-viral defense signals and a pro-inflammatory environment compared to
82 infection with influenza A virus (IAV) (4). Furthermore, in severe and critically ill COVID-19 patients, an
83 impaired type I IFN response has been observed, resulting in decreased viral clearance (5). A lack of
84 an efficient type I IFN response in these patients is in part due to inborn errors of type I IFN immunity
85 (6) or circulating auto-antibodies neutralizing type I IFNs (7). Also, a recent animal study has identified
86 that type I IFN signaling is required for the recruitment of pro-inflammatory cells into the lungs
87 following SARS-CoV-2 infection (8). These findings highlight the importance of functional type I IFN
88 responses for anti-viral defenses against SARS-CoV-2.

89 Using a mouse model of SARS-CoV-2 infection, facilitated by intranasal recombinant Adeno-
90 Associated Virus (rAAV) induced expression of human angiotensin converting enzyme 2 (hACE2), this
91 study investigated the dynamics of innate immune responses to infection with SARS-CoV-2 in the
92 context of type I IFN signaling impairment. Overall, the data show that type I IFN signaling is essential
93 to induce anti-viral responses and control viral replication and disease severity during SARS-CoV-2
94 infection. Furthermore, type I IFN signaling-deficient mice show dysregulated innate immune
95 responses to SARS-CoV-2 infection, marked by increased neutrophil recruitment into the airways and
96 delayed recruitment of myeloid inflammatory cells.

97

98 Results and discussion

99 To investigate the dynamics of innate, anti-viral immune responses to SARS-CoV-2 infection in the
100 context of type I IFN-signaling deficiency, 8–12-week-old C57BL/6 wildtype (WT) or *interferon alpha*
101 *receptor-1*^{-/-} (*Ifnar1*^{-/-}) mice were intranasally transduced with rAAV9 containing either *hACE2* or *eGFP*
102 (control) as published recently (9), followed by intranasal infection with 2x10⁶ PFU SARS-CoV-2

1
2
3 103 (D614G, first wave isolate) 20 days later and study endpoints were at 2, 4 and 8 days post infection
4 104 (d.p.i.) (Figure 1A). Gene expression analysis of *hACE2* in lung tissue 20 days post administration of
5 105 rAAV9 (before infection) showed similar expression in WT and *Ifnar1*^{-/-} mice relative to *Gapdh* (Figure
6 106 1B). Cryo-sectioning of lung tissue 20 days post administration of rAAV9-*eGFP* (before infection)
7 107 furthermore showed similar distribution of *eGFP* in WT and *Ifnar1*^{-/-} mice (Supp. Figure 1A), suggesting
8 108 similar rAAV transduction efficacy in both groups of mice. Upon infection with SARS-CoV-2, *hACE2*-
9 109 *Ifnar1*^{-/-} mice showed increased weight loss, peaking at 6 d.p.i., compared with *hACE2*-WT mice (Figure
10 110 1C). Furthermore, plaque assays on Vero cells overexpressing SARS-CoV-2 binding receptors ACE2 and
11 111 transmembrane protease serine 2 precursor TMPRSS2 (VAT cells) showed that IFNAR1-deficiency
12 112 results in significantly higher viral loads at day 2 and 4 post infection with SARS-CoV-2 compared to
13 113 *hACE2*-WT mice (Figure 1D). Gene expression of SARS-CoV-2 nucleocapsid (N) and envelope (E) genes
14 114 was significantly higher in *hACE2-Ifnar1*^{-/-} mice compared with *hACE2*-WT mice from 2 d.p.i. (Figure 1E
15 115 and Supp. Figure 2B). Since AAV-*eGFP* transduced *Ifnar1*^{-/-} mice did not become infected with SARS-
16 116 CoV-2 and did overall not differ significantly from AAV-*eGFP* transduced WT mice (Supp. Figure 2), this
17 117 group was not included in all experiments to reduce animal numbers. Together, these data show
18 118 increased viral load in *hACE2* expressing IFNAR1-deficient mice upon SARS-CoV-2 infection, measured
19 119 both by plaque assay and N and E gene expression. Previous studies have shown similar trends (8),
20 120 although differences between WT and *Ifnar1*^{-/-} are more pronounced in the model used here. This
21 121 could be due to several factors: here, Vero cells overexpressing *hACE2* and TMPRSS2 were used for
22 122 plaque assays, allowing for better viral replication, while the isolate used for infection was hCoV-
23 123 19/England/IC19/2020, which harbors the D614G spike mutation as opposed to USA-WA1/2020,
24 124 enhancing viral replication (10). Together, these factors might explain why we detected higher viral
25 125 loads and more prominent differences emerged between *hACE2*-WT and *hACE2-Ifnar1*^{-/-} mice.

26
27
28
29
30
31
32
33
34
35
36
37
38
39
40
41
42
43 126 To investigate the impact of impaired type I IFN signaling during SARS-CoV-2 infection, we first
44 127 assessed type I IFN expression upon infection. At 2 d.p.i. both IFN- α and IFN- β were significantly
45 128 increased in BAL fluid of *hACE2*-WT compared to *eGFP*-WT mice (Supp. Figure 1B). In the *hACE2-Ifnar1*^{-/-}
46 129 group, expression of IFN- α was significantly lower, while IFN- β levels were higher compared to the
47 130 *hACE2*-WT group. We next investigated ISG expression after SARS-CoV-2 infection, since in *Ifnar1*^{-/-}
48 131 mice limited amounts of type I IFN cytokines can be produced but cannot signal for downstream ISGs
49 132 induction. Chemokine *Cxcl10* and anti-viral effectors *Mx1*, *Oas1* and *Viperin* were quantified. The
50 133 expression of these ISGs was increased in *hACE2*-WT mice upon infection with SARS-CoV-2 at 2 d.p.i.,
51 134 however in *hACE2-Ifnar1*^{-/-} mice, ISG expression was significantly reduced, but not completely absent
52 135 (Figure 1F and Supp. Figure 3 C-F). These results suggest an initial increase of IFN- β in *hACE2-Ifnar1*^{-/-}
53 136 mice, which may be due to higher viral titers, but that is not translated into ISG expression due to the

1
2
3 137 lack of signaling through the IFNAR1. We therefore investigated the expression of type III IFNs, IFN-
4 138 λ 2-3, which can contribute to ISG expression. IFN- λ expression was induced upon infection in *hACE2*-
5 139 WT mice at 2 d.p.i. while remained at baseline levels in the *hACE2-Ifnar1*^{-/-} mice (Supp. Figure 1C).
6
7
8 140 Furthermore, *Ifng* gene expression was significantly increased in *hACE2-Ifnar1*^{-/-} mice later during the
9 141 infection, by 4 d.p.i. (Supp. Figure 4A). This correlated with CD3⁺ T cell recruitment to the airways
10 142 (Supp. Figure 4B-D). Our data suggest that limited levels of type I or III IFNs are produced early during
11 143 infection in the *Ifnar1*^{-/-} mice resulting in some ISG expression but overall, these data suggest that type
12 144 I IFN signaling is the main driver for inducing cell intrinsic anti-viral responses.
13
14
15
16
17 145

18 146 We next assessed the gene expression of inflammatory mediators and found that expression of the
19 147 chemokine *Cxcl1*, which is not dependent on type I IFN signaling (3), was increased in *hACE2-Ifnar1*^{-/-}
20 148 mice at 2 and 4 d.p.i. compared to *hACE2*-WT (Figure 2A and Supp. Figure 3G). As CXCL1 plays an
21 149 essential role in early host immune responses by recruiting neutrophils (11), we next analysed
22 150 infiltration of neutrophils (gated as live, CD45⁺, Ly6G⁺, Supp. Figure 5A) into the airways at 2 d.p.i. In
23 151 line with highly increased gene expression of *Cxcl1*, neutrophil recruitment to the airways (BAL) was
24 152 significantly increased in *hACE2-Ifnar1*^{-/-} mice at 2 d.p.i., both proportional of leukocytes (CD45⁺ cells)
25 153 and in total numbers (Figure 2B and C). This was recapitulated in lung tissue with increased
26 154 proportions of neutrophils in type I IFN signaling-impaired mice at 2 d.p.i. (Figure 2D and Supp. Figure
27 155 3H), decreasing over time. Taken together, these findings suggest that during SARS-CoV-2 infection,
28 156 type I IFN signaling deficiency results in increased neutrophil recruitment via CXCL1, thereby
29 157 contributing to a pro-inflammatory environment. Indeed, *Cxcl1* is also increased in *Ifnar1*^{-/-} mice during
30 158 influenza A with secondary pneumococcal infection (12), but decreased during RSV infection in mice
31 159 (13), highlighting a pathogen specific CXCL1 response. Furthermore, since we show similar trends for
32 160 viral load and neutrophil recruitment upon SARS-CoV-2 infection (both significantly increased in
33 161 *hACE2-Ifnar1*^{-/-} mice), which is a mechanism present in other respiratory viral infections such as
34 162 respiratory syncytial virus (RSV) (13, 14), it will be important to further investigate the link between
35 163 neutrophil recruitment and viral load in this model.
36
37
38
39
40
41
42
43
44
45
46
47
48
49

50 165 Since monocyte recruitment to the airways and lungs is key to early host responses to viral infection,
51 166 we next investigated the expression of monocyte recruiting chemokine CCL2 and the recruitment of
52 167 inflammatory myeloid cells. CCL2 protein expression was increased in BAL fluid of *hACE2*-WT mice at
53 168 2 d.p.i. with SARS-CoV-2 (Supp. Figure 3I). However, in *hACE2-Ifnar1*^{-/-} mice CCL2 expression was
54 169 significantly lower at 2 d.p.i., peaking at 4 d.p.i. at lower levels than in IFNAR1-sufficient mice (Figure
55 170 3A). These findings are in line with a report identifying early CCR2 signaling essential to restrict viral
56
57
58
59
60

1
2
3 171 burden in the lung in a mouse model of SARS-CoV-2 infection (15). The recruitment of CD64⁺CD11b⁺
4
5 172 inflammatory myeloid cells to the lung followed similar kinetics, as in *hACE2*-WT mice proportions
6
7 173 were highest at 2 d.p.i. and subsequently decreased, while in IFNAR1-deficient mice proportions and
8
9 174 total numbers of CD64⁺CD11b⁺ inflammatory myeloid cells strongly increased between 2 and 4 d.p.i.
10
11 175 and were highest at 8 d.p.i. (Figure 3B and Supp. Figure 3J). We next assessed expression of the
12
13 176 monocyte/macrophage differentiation antigen Ly6C within this population, since previous studies
14
15 177 reported the infiltration of CD64⁺CD11b⁺Ly6C⁺ inflammatory myeloid cells into the lung during SARS-
16
17 178 CoV-2 infection (8, 15). This showed highly increased proportions of CD64⁺CD11b⁺Ly6C⁺ in *hACE2*-WT
18
19 180 but not IFNAR1-deficient mice at 2 d.p.i. in the BAL (Supp. Figure 5D) and lung (Figure 3C-D and Supp.
20
21 181 Figure 3K), suggesting type I IFN dependency for recruitment. However, as we have previously shown
22
23 182 that Ly6C is gradually downregulated on monocytes during response to respiratory viral infection (16),
24
25 183 we also analyzed CD64⁺CD11b⁺ Ly6C⁻ cells. The presence of CD64⁺CD11b⁺ Ly6C⁻ inflammatory myeloid
26
27 184 cells in the airways was not type I IFN signaling dependent, since both proportions and total numbers
28
29 185 were significantly increased in *hACE2-Ifnar1*^{-/-} mice at 4 and 8 d.p.i. (Figure 3C and E), while at 2 d.p.i.
30
31 186 in the airways no significant differences emerged (Supp. Figure 5F). This accounts for the delayed
32
33 187 emergence of inflammatory myeloid cells in the lung during type I IFN signaling impairment shown in
34
35 188 Figure 3B and overall indicates altered recruitment dynamics of inflammatory myeloid cells. Taking
36
37 189 these data together, our model recapitulates the deficiency of type I interferon responses seen in
38
39 190 severe SARS-CoV-2 infection, which in patients is marked by decreased IFN- α , type I IFN activity and
40
41 191 ISG score, as well as neutrophilia and increased CCL2 (5). Our data suggest that the lack of type I IFN
42
43 192 signaling results in dysregulated innate immune responses in the lung during SAR-CoV-2 infection.

40 193 **Concluding Remarks**

42 194 In summary, using a mouse model of SARS-CoV-2 infection we show that type I IFN signaling is
43
44 195 essential for inducing anti-viral effector responses, control of virus replication and disease severity.
45
46 196 Our data indicate that type I IFN signaling-deficient mice express increased levels of *Cxcl1* in the lung
47
48 197 and increased infiltration of neutrophils to the airways compared to WT controls. Furthermore, we
49
50 198 found reduced and delayed production of CCL2 and altered recruitment of inflammatory myeloid cells
51
52 199 during IFNAR1-deficiency. This, together with an increased viral burden is associated with more severe
53
54 200 disease in type I IFN signaling-deficient mice. The data shown here will be valuable for better
55
56 201 understanding how impaired type I IFN signaling drives SARS-CoV-2 pathology and disease severity,
57
58 202 which is highly relevant considering the large contribution of impaired type I IFN responses on life-
59
60 203 threatening SARS-CoV-2 infections (6, 7) and deaths (17) and for the development of type I IFN-based
204
205 treatment options for COVID-19 in vulnerable populations. To conclude, our findings show that type I

205 IFN deficiency results in dysregulated innate immune responses to SARS-CoV-2 infection in the rAAV-
206 *hACE2* mouse model.

207 **Materials and Methods**

208 **Mice**

209 C57BL/6 mice were purchased from Charles River UK Inc. *Ifnar1*^{-/-} mice on a C57BL/6 background were
210 bred in-house. All mice were bred and maintained in pathogen-free conditions and 8–12-week-old
211 mice were used for experiments. All animal experiments were reviewed and approved by the Animal
212 Welfare and Ethical Review Board (AWERB) at Imperial College London and approved by the UK Home
213 Office in accordance with the Animals Act 1986 (Scientific Procedures) and ARRIVE guidelines. Both
214 male and female mice were used for experiments after excluding sex bias in preliminary experiments.
215 All experiments were performed twice, independently, per time point.

216

217 **rAAV vector production**

218 The production, purification, and titration of rAAV2/9-*eGFP* or *hACE2* vectors were performed as
219 previously described (9). Briefly, the respective rAAV vector was produced by polyethylenimine (PEI,
220 PolySciences)-based triple transfection of human embryonic kidney (HEK) 293T/17 cells (ATCC, CRL-
221 11268). The AAV plasmids transfected included the Adenovirus helper plasmid (pAdDeltaF6), AAV
222 Rep-Cap pAAV2/9 plasmid and the transgene plasmid. The transgene plasmid containing *eGFP* or
223 *hACE2* was engineered to include a lung-optimized hCEFI (human Cytomegalovirus
224 enhancer/elongation factor 1 alpha) promoter (18), Woodchuck Hepatitis Virus Post-transcriptional
225 Regulatory Element (WPRE) (19) and mir142-3pT (20). rAAV particles were concentrated and
226 formulated into PBS using 100 kDa Ultra centrifugal filters (Amicon, Merck) after iodixanol gradient
227 centrifugation. Physical titre (DNase-resistant genome copies, DRGC/mL) was determined by
228 quantitative polymerase chain reaction (qPCR) analysis with primers and a probe against WPRE (21).
229 Purity of vectors was confirmed by analyzing 20 µl of diluted vector on 4-12% SDS polyacrylamide gels,
230 where total protein was visualized using Coomassie stain according to the manufacturer's protocols
231 (Life Technologies).

232

233 **hACE2 transduction**

234 For transduction, WT or *Ifnar1*^{-/-} mice were lightly anesthetized and instilled i.n. with 1x10¹¹ DNase
235 Resistant Gene Copies (DRGC) rAAV9-*eGFP* or rAAV9-*hACE2* in 100 µl PBS. *hACE2* gene expression in
236 whole lung homogenate was assessed at day 20 post instillation by relative quantification to *Gapdh*
237 using primers and probes for *hACE2* listed in the key resource table.

238

239 **Cryosectioning and native eGFP detection**

240 Mice were sacrificed 20 days post instillation of AAV-eGFP or PBS and lungs were removed after
241 inflation with 4% PFA. After 24-hour fixation in 4% PFA, lungs were inflated with 30% sucrose and
242 submerged in 30% sucrose for 24 hours. Lungs were subsequently inflated with 1:1 cryo embedding
243 matrix (OCT)/30% sucrose and individual lobes were submerged in OCT/30% sucrose in plastic molds
244 and frozen at -80 °C. Left lungs were cryosectioned to produce 7 µm thick sections, mounted using
245 DAPI-supplemented mounting media with coverslip, and eGFP expression was detected by fluorescent
246 microscopy using the EVOS FL Auto 2 system (Thermo Scientific).

247

248 **Virus and infections**

249 First wave SARS-CoV-2 (D614G, isolate of hCoV-19/England/IC19/2020) was grown in African green
250 monkey kidney cells overexpressing human ACE2 and TMPRSS2 (Vero-ACE2-TMPRSS2; VAT cells) (22).
251 For infection 20 days post transduction with rAAVs, mice were lightly anesthetized and instilled i.n.
252 with 2×10^6 plaque forming units (PFU) of SARS-CoV-2 in 100 µl volume. SARS-CoV-2 titre was assessed
253 in lungs at 2, 4 and 8 d.p.i. using a plaque assay. In brief, serial dilutions of lung homogenate in serum-
254 free Dulbecco's Modified Eagle Medium (DMEM, containing 1% non-essential amino acids (NEAA),
255 100U/ml Penicillin and 100 µg/ml Streptomycin) were performed and inoculated onto VAT cells for 1
256 h at 37°C. The inoculum was then removed and replaced with overlay medium (1x MEM, 0.2% w/v
257 BSA, 0.16% w/v NaHCO₃, 10 mM HEPES, 2 mM L-Glutamine, 100 U/ml penicillin, 100 µg/ml
258 streptomycin and 0.84% agarose). Plates were incubated for 3 days at 37°C before overlay was
259 removed and cells were stained for 1 h at room temperature in 2x crystal violet solution. Virus plaques
260 were counted and multiplied by the dilution factor to calculate titer as PFU/ml.

261

262 **Isolation of lung cells**

263 Mice were sacrificed at 0.75, 2, 4 and 8 d.p.i. and lungs were perfused with PBS. To obtain lung
264 leukocytes, lung lobes were cut into smaller pieces and incubated in complete DMEM (cDMEM,
265 supplemented with 10% fetal bovine serum, 2mM L-glutamine, 100 U/ml penicillin and 100 µg/ml
266 streptomycin), 1mg/ml Collagenase D (Roche) and 30 µg/ml DNase I (Invitrogen) for 1h at 37°C and
267 then mashed through a 100-µm filter (BD). Red blood cells were lysed using Ammonium-Chloride-
268 Potassium buffer.

269

270 **BAL cell processing**

271 BAL was collected by flushing the lungs three times with 1 ml PBS supplemented with 5 mM EDTA (Life
272 Technologies). BAL cells and supernatant were separated by centrifugation and BAL supernatants

1
2
3 273 were exposed to UV light for 2 min to inactivate SARS-CoV-2. Red blood cells were lysed using
4 274 Ammonium-Chloride-Potassium buffer.

5
6 275

7 8 276 **Flow cytometry**

9
10 277 After red blood cell lysis, lung and BAL cells were incubated for 30 min with fixable live-dead Aqua dye
11 278 (Invitrogen), followed by fixation for 30 minutes with 4% paraformaldehyde (PFA) to inactivate virus.
12
13 279 Cells were then incubated for 20 min with a purified rat IgG_{2b} anti-mouse CD16/CD32 receptor
14
15 280 antibody (BD) to block Fc binding, followed by staining with fluorochrome-conjugated antibodies
16
17 281 against CD45 (30-F11, BV605), CD26 (H194-112, BV711), Siglec-F (E50-2440, BV786), Ly6G (1A8,
18 282 AF488), Ly6C (12HK1.4, PE), CD11c (HL3, PE-CF594), CD64 (X54-5/7.1, APC) and CD11b (M1/70, AF700)
19
20 283 in PBS containing 1% BSA and 5 mM EDTA for 25 min at 4°C. For the adaptive immune cells, they were
21
22 284 stained with CD11c (HL3, V450), Siglec-F (E50-2440, BV786), CD19 (6D5, AF488), CD45 (30-F11, PerCP-
23 285 Cy5.5), Ly6G (1A8, PE-Cy7) and CD3 (17A2, AF700). Samples were analysed on a BD-Fortessa Flow
24
25 286 Cytometer equipped with 50-mW 504-nm, 50-mW 488-nm, 50-mW 561-nm and 20-mW 633-nm lasers
26
27 287 and an ND1.0 filter in front of the FSC photodiode. All antibodies were purchased from BD, Biolegend
28
29 288 or eBioscience. Data were analyzed with FlowJo software (Tree Star).

30 289

31 32 290 **RNA isolation and quantitative RT-PCR**

33 291 Lung tissue was homogenized in TRIzol and RNA extraction performed according to manufacturer's
34 292 instructions. After the chloroform step, the aqueous phase containing RNA was further processed
35 293 using the RNeasy Mini Kit (QIAGEN) according to manufacturer's instructions. 2 µg RNA was reverse
36
37 294 transcribed using a High-Capacity RNA-to-cDNA kit (Applied Biosystems) according to manufacturer's
38
39 295 instructions. To quantify mRNA levels in lung tissue, quantitative RT-PCR reactions for *Oas1*, *Viperin*
40 296 and *Ifnl* were performed using primers and probes as previously described (23). Analysis was
41
42 297 performed using the QuantiTect Probe PCR Master Mix (QIAGEN) and the 7500 Fast real-Time PCR
43
44 298 System (Applied Biosystems). For absolute quantification, the exact number of copies of the gene of
45
46 299 interest was calculated using a plasmid DNA standard curve, and the results were normalized to levels
47
48 300 of *Gapdh* (Applied Biosystems). For relative quantification, the expression of *Cxcl1*, *Cxcl10*, *hACE2*,
49
50 301 *Mx1* and SARS-CoV-2 *N* and *E* gene was expressed relatively to the expression of *Gapdh*. First, the Δ CT
51
52 302 (CT = cycle threshold) between the target gene and *Gapdh* was calculated for each sample, followed
53
54 303 by calculation of $2^{-\Delta$ CT. Analysis was performed using 7500 Fast System SDS Software (Applied
55
56 304 Biosystems).

57 305

58 306 **Chemokine and IFN detection**

1
2
3 307 CCL2 and IFN- λ 2/3 quantifications were performed on BAL fluid using mouse DuoSet ELISA (R&D
4 308 Systems) according to the manufacturer's instructions. Data were acquired on a SpectraMax Plus plate
5 309 reader (Molecular Devices) and analysed using SoftMax software (version 5.2). The concentration of
6 310 IFN- α and IFN- β was measured in BAL fluid using the Mouse ProCartaPlex Immunoassay (Invitrogen)
7 311 according to the manufacturer's instructions. Data were acquired and analysed with a Bio-Plex 200
8 312 system (Bio-Rad Laboratories).
9

10 313

11 314 **Statistical analysis**

12 315 Statistical analysis was performed using Prism 9.2 (Graph-Pad Software). One-way ANOVA with
13 316 Tukey's post-hoc test was used to compare multiple groups. Data are expressed as mean \pm SEM, and
14 317 for all tests a value of $P < 0.05$ was considered significant. * $P < 0.05$, ** $P < 0.01$, *** $P < 0.005$, ****
15 318 $P < 0.001$
16

17 319

18 320 **Acknowledgements**

19 321 C. J. is supported by grants from UKRI-BBSRC (BB/V013831/1), Rosetrees Trust and Stoneygate Trust
20 322 (M370 and M370-F1), Rosetrees Trust and The John Black Charitable Foundation (M956) and the
21 323 Imperial College COVID-19 research fund. W.S.B., J.Z. and J.C.B are supported by the G2P-UK National
22 324 Virology consortium funded by MRC/UKRI (grant ref: MR/W005611/1.). D.R.G., S.C.H. and Y.D are
23 325 supported by a Wellcome Trust Portfolio grant (110579/Z/15/Z). For the purpose of open access, the
24 326 authors have applied a CC BY public copyright license to any Author Accepted Manuscript version
25 327 arising from this submission. The graphical abstract has been created using Biorender.com. We also
26 328 thank the staff of St Mary's flow cytometry facility and the St Mary's animal facility for their assistance
27 329 and members of the Johansson lab for scientific discussions.
28

29 330

30 331 **Author contribution**

31 332 P.P.O. designed, performed, and analyzed the experiments and wrote the paper. M.G.M. and C.M.
32 333 performed specific experiments and reviewed the paper. Y.D., D.R.G., S.C.H., O.H., and K.M.M.
33 334 designed, manufactured and provided rAAV9-*hACE2* and rAAV9-*eGFP* and reviewed the paper,
34 335 additionally Y.D. and K.M.M. performed specific experiments. J.Z., J.C.B. and W.S.B. provided advice
35 336 and the SARS-CoV-2 WT isolate (D614G) and reviewed the paper. C.J. supervised the project, designed
36 337 the experiments, and wrote the paper.
37

38 338

39 339 **Conflict of interest**

40 340

1
2
3 340 The authors declare no commercial or financial conflict of interest.
4
5 341

6
7 342 **Data availability statement**
8

9 343 The data that support the findings of this study are available from the corresponding author upon
10 344 reasonable request.
11
12
13

14 345 **Ethics approval**
15

16
17 346 All animal experiments were reviewed and approved by the Animal Welfare and Ethical Review Board
18 (AWERB) at Imperial College London and approved by the UK Home Office in accordance with the
19 347 Animals (Scientific Procedures) Act 1986 Amendment Regulations (PPL P3AFFFODD Johansson).
20 348
21
22

23 349 **References**
24

- 25 350 1. O'Driscoll M, Ribeiro Dos Santos G, Wang L, Cummings DAT, Azman AS, Paireau J, Fontanet A,
26 351 Cauchemez S, Salje H. Age-specific mortality and immunity patterns of SARS-CoV-2. *Nature*
27 352 2021;590:140–145.
28
29 353 2. Platanias LC. Mechanisms of type-I- and type-II-interferon-mediated signalling. *Nature*
30 354 *Reviews Immunology* 2005;5:375–386.
31
32 355 3. Trinchieri G. Type I interferon: Friend or foe? *Journal of Experimental Medicine*
33 356 2010;207:2053–2063.
34
35 357 4. Blanco-Melo D, Nilsson-Payant BE, Liu WC, Uhl S, Hoagland D, Møller R, Jordan TX, Oishi K,
36 358 Panis M, Sachs D, Wang TT, Schwartz RE, Lim JK, Albrecht RA, tenOever BR. Imbalanced Host
37 359 Response to SARS-CoV-2 Drives Development of COVID-19. *Cell* 2020;181:1036-1045.e9.
38
39 360 5. Hadjadj J, Yatim N, Barnabei L, Corneau A, Boussier J, Smith N, Péré H, Charbit B, Bondet V,
40 361 Chenevier-Gobeaux C, Breillat P, Carlier N, Gauzit R, Morbieu C, Pène F, Marin N, Roche N,
41 362 Szwabel T-A, Merklings SH, Treluyer J-M, Veyer D, Mouthon L, Blanc C, Tharaux P-L, Rozenberg
42 363 F, Fischer A, Duffy D, Rieux-Laucat F, Kernéis S, *et al.* Impaired type I interferon activity and
43 364 inflammatory responses in severe COVID-19 patients. *Science (1979)* 2020;369:718–724.
44
45 365 6. Zhang Q, Liu Z, Moncada-Velez M, Chen J, Ogishi M, Bigio B, Yang R, Arias AA, Zhou Q, Han JE,
46 366 Ugurbil AC, Zhang P, Rapaport F, Li J, Spaan AN, Boisson B, Boisson-Dupuis S, Bustamante J,
47 367 Puel A, Ciancanelli MJ, Zhang SY, Béziat V, Jouanguy E, Abel L, Cobat A, Casanova JL, Bastard
48 368 P, Korol C, Rosain J, *et al.* Inborn errors of type I IFN immunity in patients with life-
49 369 threatening COVID-19. *Science (1979)* 2020;370:.
50
51 370 7. Bastard P, Rosen LB, Zhang Q, Michailidis E, Hoffmann HH, Zhang Y, Dorgham K, Philippot Q,
52 371 Rosain J, Béziat V, Manry J, Shaw E, Haljasmägi L, Peterson P, Lorenzo L, Bizien L, Trouillet-
53 372 Assant S, Dobbs K, de Jesus AA, Belot A, Kallaste A, Catherinot E, Tandjaoui-Lambiotte Y, le
54 373 Pen J, Kerner G, Bigio B, Seeleuthner Y, Yang R, Bolze A, *et al.* Autoantibodies against type I
55 374 IFNs in patients with life-threatening COVID-19. *Science (1979)* 2020;370:.
56
57
58
59
60

- 1
2
3 375 8. Israelow B, Song E, Mao T, Lu P, Meir A, Liu F, Alfajaro MM, Wei J, Dong H, Homer RJ, Ring A,
4 376 Wilen CB, Iwasaki A. Mouse model of SARS-CoV-2 reveals inflammatory role of type I
5 377 interferon signaling. *Journal of Experimental Medicine* 2020;217:.
- 7 378 9. Du Y, Miah KM, Habib O, Meyer-Berg H, Conway CC, Viegas MA, Dean R, Satyapertiwi D, Zhao
8 379 J, Wang Y, Temperton NJ, Gamlen TPE, Gill DR, Hyde SC. Lung directed antibody gene transfer
9 380 confers protection against SARS-CoV-2 infection. *Thorax* 2022;thoraxjnl-2021-
11 381 217650.doi:10.1136/thoraxjnl-2021-217650.
- 13 382 10. Plante JA, Liu Y, Liu J, Xia H, Johnson BA, Lokugamage KG, Zhang X, Muruato AE, Zou J, Fontes-
14 383 Garfias CR, Mirchandani D, Schariton D, Bilello JP, Ku Z, An Z, Kalveram B, Freiberg AN,
15 384 Menachery VD, Xie X, Plante KS, Weaver SC, Shi PY. Spike mutation D614G alters SARS-CoV-2
16 385 fitness. *Nature* 2021;592:116–121.
- 18 386 11. Johansson C, Kirsebom FCM. Neutrophils in respiratory viral infections. *Mucosal Immunology*
19 387 2021;14:815–827.
- 21 388 12. Shahangian A, Chow EK, Tian X, Kang JR, Ghaffari A, Liu SY, Belperio JA, Cheng G, Deng JC.
22 389 Type I IFNs mediate development of postinfluenza bacterial pneumonia in mice. *Journal of*
23 390 *Clinical Investigation* 2009;119:1910–1920.
- 25 391 13. Goritzka M, Durant LR, Pereira C, Salek-Ardakani S, Openshaw PJM, Johansson C. Alpha/Beta
26 392 Interferon Receptor Signaling Amplifies Early Proinflammatory Cytokine Production in the
27 393 Lung during Respiratory Syncytial Virus Infection. *Journal of Virology* 2014;88:6128–6136.
- 29 394 14. Goritzka M, Pereira C, Makris S, Durant LR, Johansson C. T cell responses are elicited against
30 395 Respiratory Syncytial Virus in the absence of signalling through TLRs, RLRs and IL-1R/IL-18R.
31 396 *Scientific Reports* 2015;5:.
- 33 397 15. Vanderheiden A, Thomas J, Soung AL, Davis-Gardner ME, Floyd K, Jin F, Cowan DA, Pellegrini
34 398 K, Shi PY, Grakoui A, Klein RS, Bosinger SE, Kohlmeier JE, Menachery VD, Suthar MS. CCR2
35 399 Signaling Restricts SARS-CoV-2 Infection. *mBio* 2021;12:1–14.
- 37 400 16. Goritzka M, Makris S, Kausar F, Durant LR, Pereira C, Kumagai Y, Culley FJ, Mack M, Akira S,
38 401 Johansson C. Alveolar macrophage-derived type I interferons orchestrate innate immunity to
39 402 RSV through recruitment of antiviral monocytes. *Journal of Experimental Medicine*
40 403 2015;212:699–714.
- 42 404 17. Bastard P, Gervais A, Voyer T Le, Rosain J, Philippot Q, Manry J, Michailidis E, Hoffmann HH,
43 405 Eto S, Garcia-Prat M, Bizien L, Parra-Martínez A, Yang R, Haljasmägi L, Migaud M, Särekannu
44 406 K, Maslovskaia J, De Prost N, Tandjaoui-Lambiotte Y, Luyt CE, Amador-Borrero B, Gaudet A,
45 407 Poissy J, Morel P, Richard P, Cognasse F, Troya J, Trouillet-Assant S, Belot A, *et al.*
46 408 Autoantibodies neutralizing type I IFNs are present in ~4% of uninfected individuals over 70
47 409 years old and account for ~20% of COVID-19 deaths. *Science Immunology* 2021;6:.
- 49 410 18. Hyde SC, Pringle IA, Abdullah S, Lawton AE, Davies LA, Varathalingam A, Nunez-Alonso G,
50 411 Green AM, Bazzani RP, Sumner-Jones SG, Chan M, Li H, Yew NS, Cheng SH, Christopher Boyd
51 412 A, Davies JC, Griesenbach U, Porteous DJ, Sheppard DN, Munkonge FM, Alton EFWF, Gill DR.
52 413 CpG-free plasmids confer reduced inflammation and sustained pulmonary gene expression.
53 414 *Nature Biotechnology* 2008;26:549–551.
- 55 415 19. Zanta-Boussif MA, Charrier S, Brice-Ouzet A, Martin S, Opolon P, Thrasher AJ, Hope TJ, Galy A.
56 416 Validation of a mutated PRE sequence allowing high and sustained transgene expression

- 417 while abrogating WHV-X protein synthesis: Application to the gene therapy of WAS. *Gene*
418 *Therapy* 2009;16:605–619.
- 419 20. Brown BD, Venneri MA, Zingale A, Sergi LS, Naldini L. Endogenous microRNA regulation
420 suppresses transgene expression in hematopoietic lineages and enables stable gene transfer.
421 *Nature Medicine* 2006;12:585–591.
- 422 21. Meyer-Berg H, Zhou Yang L, Pilar de Lucas M, Zambrano A, Hyde SC, Gill DR. Identification of
423 AAV serotypes for lung gene therapy in human embryonic stem cell-derived lung organoids.
424 *Stem Cell Research and Therapy* 2020;11:1–6.
- 425 22. Rihn SJ, Merits A, Bakshi S, Turnbull ML, Wickenhagen A, Alexander AJT, Baillie C, Brennan B,
426 Brown F, Bruncker K, Bryden SR, Burness KA, Carmichael S, Cole SJ, Cowton VM, Davies P,
427 Davis C, de Lorenzo G, Donald CL, Dorward M, Dunlop JI, Elliott M, Fares M, da Silva Filipe A,
428 Freitas JR, Furnon W, Gestuveo RJ, Geyer A, Giesel D, *et al.* A plasmid DNA-launched SARS-
429 CoV-2 reverse genetics system and coronavirus toolkit for COVID-19 research. *PLoS Biology*
430 2021;19:1–22.
- 431 23. Kirsebom FCM, Kausar F, Nuriev R, Makris S, Johansson C. Neutrophil recruitment and
432 activation are differentially dependent on MyD88/TRIF and MAVS signaling during RSV
433 infection. *Mucosal Immunology* 2019;12:1244–1255.

436 Figure legends

437 Figure 1: Increased viral load, weight loss and lower expression of ISGs in *Ifnar1*^{-/-} mice during 438 infection with SARS-CoV-2

439 A) Recombinant Adeno-associated virus (rAAV) containing human angiotensin converting enzyme 2
440 (*hACE2*) or *eGFP* genes was administered intranasally to *Ifnar1*^{-/-} or wildtype (WT) mice (1x10¹¹ Dnase
441 resistant gene copies/mouse). 20 days later mice were intranasally infected with SARS-CoV-2 (D614G,
442 2x10⁶ PFU/mouse). Lungs and bronchoalveolar lavage (BAL) were harvested at 2, 4 and 8 days post
443 infection (d.p.i). B) Expression of *hACE2* in lung tissue relative to *Gapdh*, measured by RT-PCR before
444 infection (d20 post transduction with rAAV). WT/rAAV-*eGFP* n = 3, *Ifnar1*^{-/-} /rAAV-*eGFP* n = 4,
445 WT/rAAV-*hACE2* n = 4, *Ifnar1*^{-/-} /rAAV-*hACE2* n = 5). C) Weight loss post infection with SARS-CoV-2. D)
446 Viral load measured by plaque assay on Vero cells overexpressing *hACE2* and *TMPRESS2*. E) Expression
447 of SARS-CoV-2 *N gene* (nucleocapsid phosphoprotein) and *E gene* (envelope protein) in lung tissue
448 relative to *Gapdh*, measured by RT-PCR. F) Gene expression analysis of IFN stimulated genes (ISG)
449 *Cxcl10*, *Mx1*, *Oas1* and *Viperin* measured by RT-PCR, relative to expression of *Gapdh* or total copy
450 numbers normalized to expression of *Gapdh* (*Oas1* and *Viperin*). Data are shown as mean ± SEM. B)
451 WT/rAAV-*eGFP* n = 3, WT/rAAV-*hACE2* n = 4, *Ifnar1*^{-/-} /rAAV-*hACE2* n = 5 C – F) Two independent
452 experiments per time point, data pooled, n = 6-8 per group. One Way ANOVA + Tukey's multiple

1
2
3 453 comparison test per time point; * indicates significant difference between WT rAAV-*hACE2* and *Ifnar1*^{-/-}
4 454 rAAV-*hACE2*, * P < 0.05, ** P < 0.01, *** p < 0.005, **** p < 0.001.

5
6 455

7
8 456 **Figure 2: Increased neutrophil recruitment to airways in IFNAR1-deficient mice during SARS-COV-2**
9 **infection**

10 457
11 458 A) Gene expression of *Cxcl1* in lung tissue relative to *Gapdh* at 2, 4 and 8 d.p.i. with SARS-CoV-2
12 459 (D614G), measured by RT-PCR. B) Proportions of live, CD45⁺ and total numbers of neutrophils in BAL
13 460 at 2 d.p.i. C) Representative flow cytometry plots of lung cells gated on live, CD45⁺ Ly6G⁺ D) Proportions
14 461 of live, CD45⁺ and total numbers of neutrophils in lung tissue at 2, 4 and 8 d.p.i. Data are shown as
15 462 mean ± SEM. Two independent experiments per time point, data pooled, n = 6-8 per group. One Way
16 463 ANOVA + Tukey's multiple comparison test per time point; * indicates significant difference between
17 464 *hACE2*-WT and *hACE2-Ifnar1*^{-/-}, * P < 0.05, ** P < 0.01, *** P < 0.005, **** P < 0.001.

18
19
20
21
22 465

23 466 **Figure 3: Type I interferon signaling deficiency results in dysregulated inflammatory myeloid cell**
24 467 **recruitment during SARS-CoV-2 infection**

25 468 A) Protein expression of CCL2 in BAL fluid at 2, 4 and 8 d.p.i. measured by ELISA. B) Proportions of live,
26 469 CD45⁺ and total numbers of CD64⁺ CD11b⁺ inflammatory myeloid cells in lung tissue at 2, 4 and 8 d.p.i.
27 470 C) Representative flow cytometry plots of lung cells gated on live, CD45⁺ Ly6G⁻ SigF⁻ CD11b⁺. D)
28 471 Proportions of live, CD45⁺ and total numbers of CD64⁺ CD11b⁺ Ly6C⁺ inflammatory myeloid cells in
29 472 lung tissue at 2, 4 and 8 d.p.i. E) Proportions of live, CD45⁺ and total numbers of CD64⁺ CD11b⁺ Ly6C⁻
30 473 inflammatory myeloid cells in lung tissue at 2, 4, and 8 d.p.i. Data are shown as mean ± SEM. Two
31 474 independent experiments per time point, data pooled, n = 6-8 per group. One Way ANOVA + Tukey's
32 475 multiple comparison test per time point; * indicates significant difference between *hACE2*-WT and
33 476 *hACE2-Ifnar1*^{-/-}, * P < 0.05, ** P < 0.01, *** P < 0.005, **** P < 0.001. Dotted line = limit of detection.

34
35
36
37
38
39
40
41
42 477

43
44
45 478
46
47
48
49
50
51
52
53
54
55
56
57
58
59
60

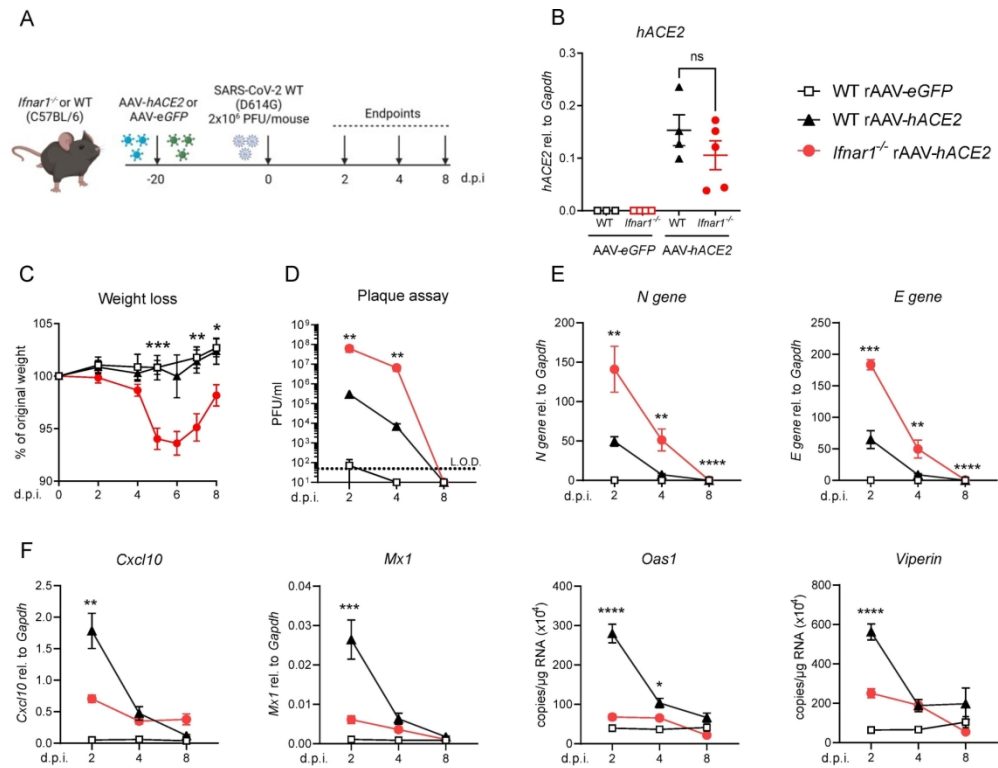


Fig1 eps format

161x122mm (300 x 300 DPI)

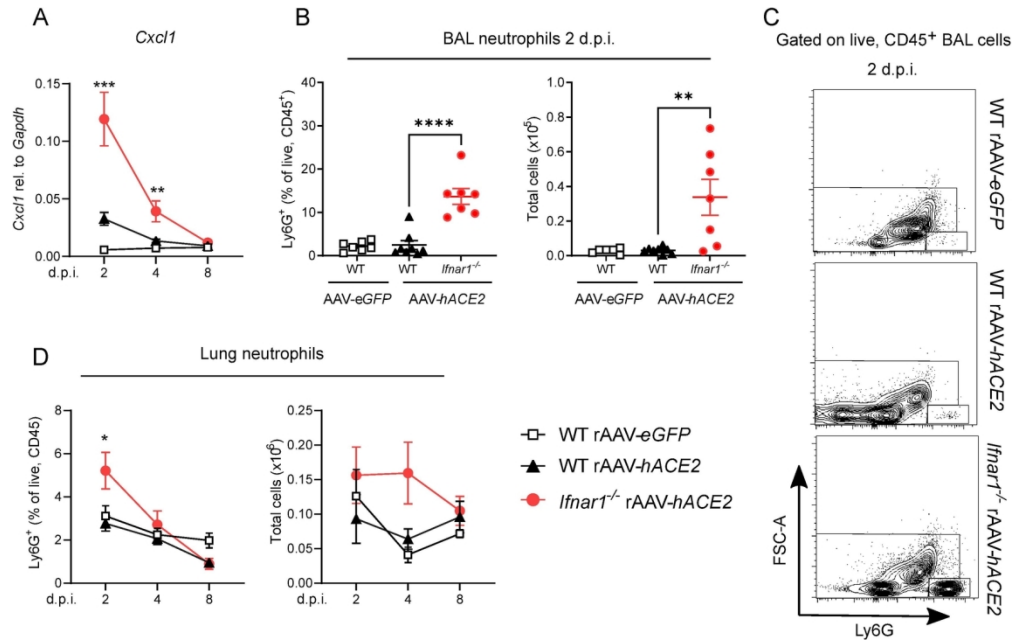


Fig2 eps format

147x93mm (300 x 300 DPI)

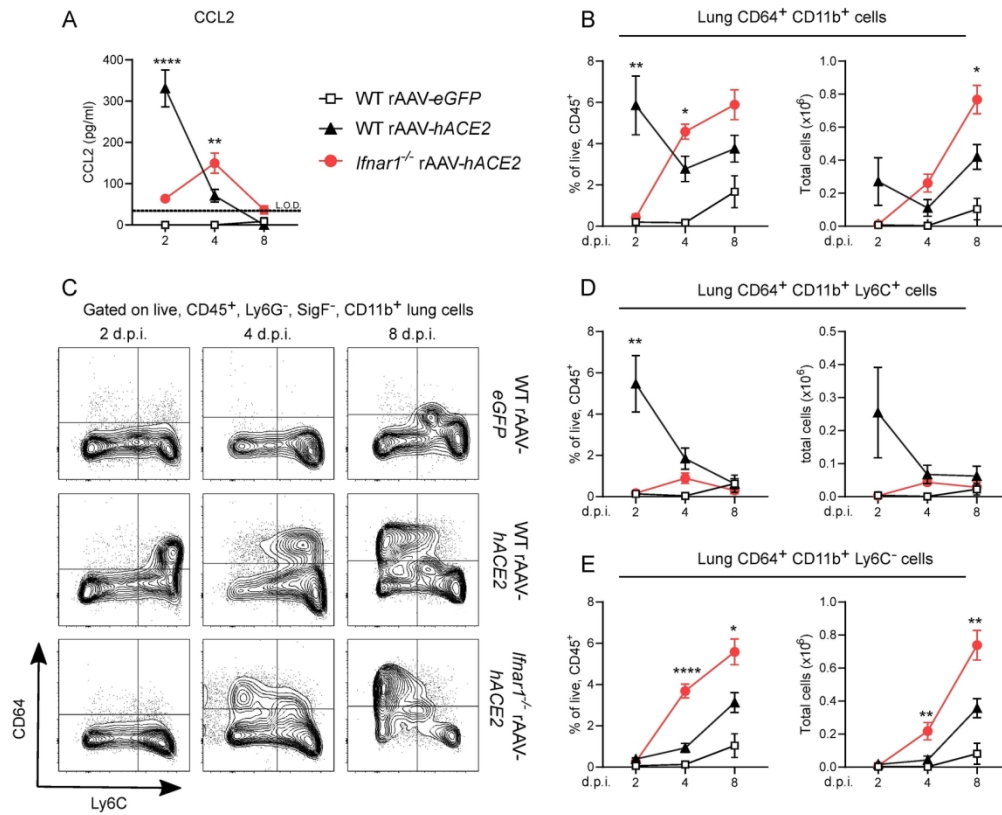
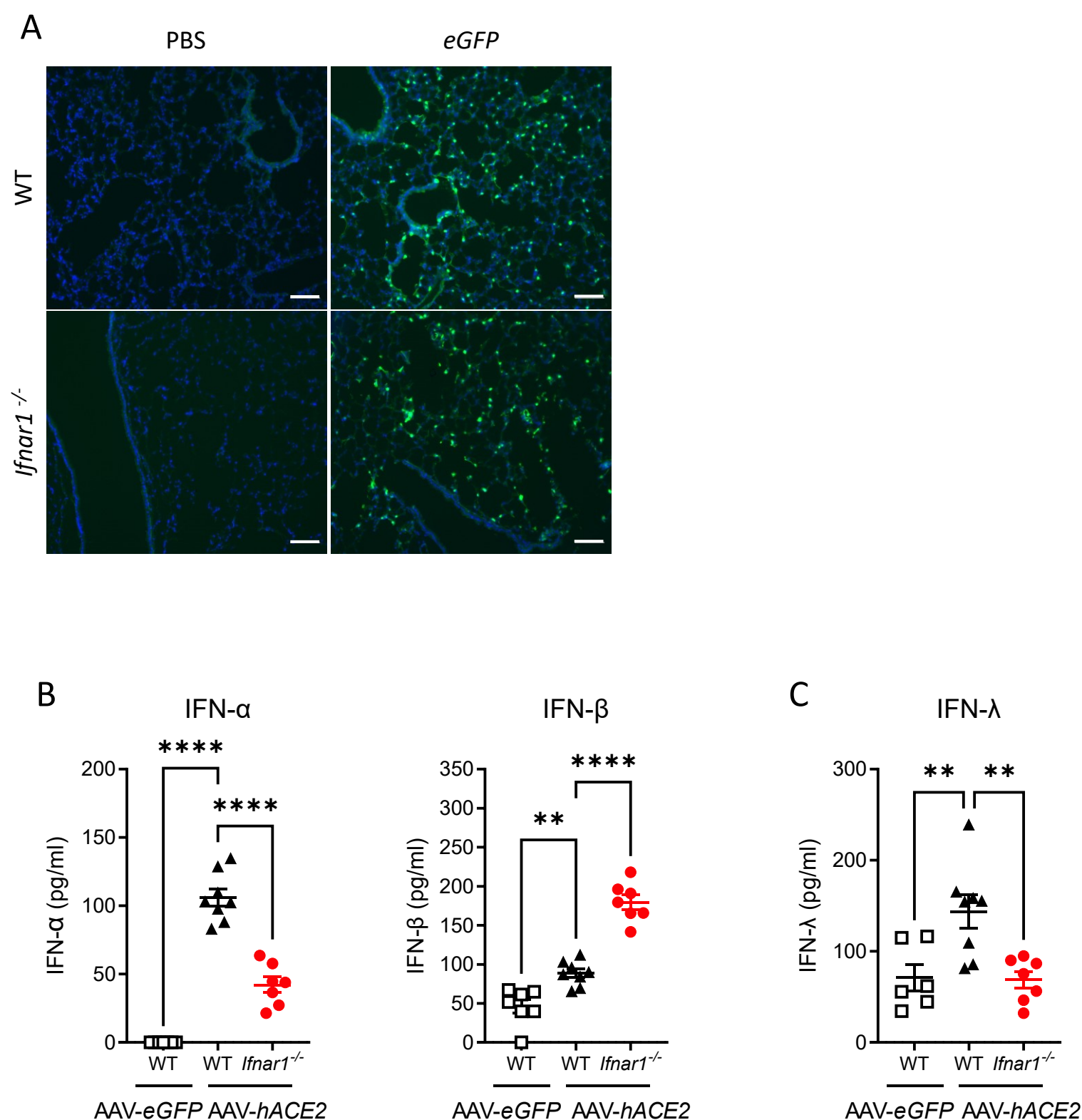


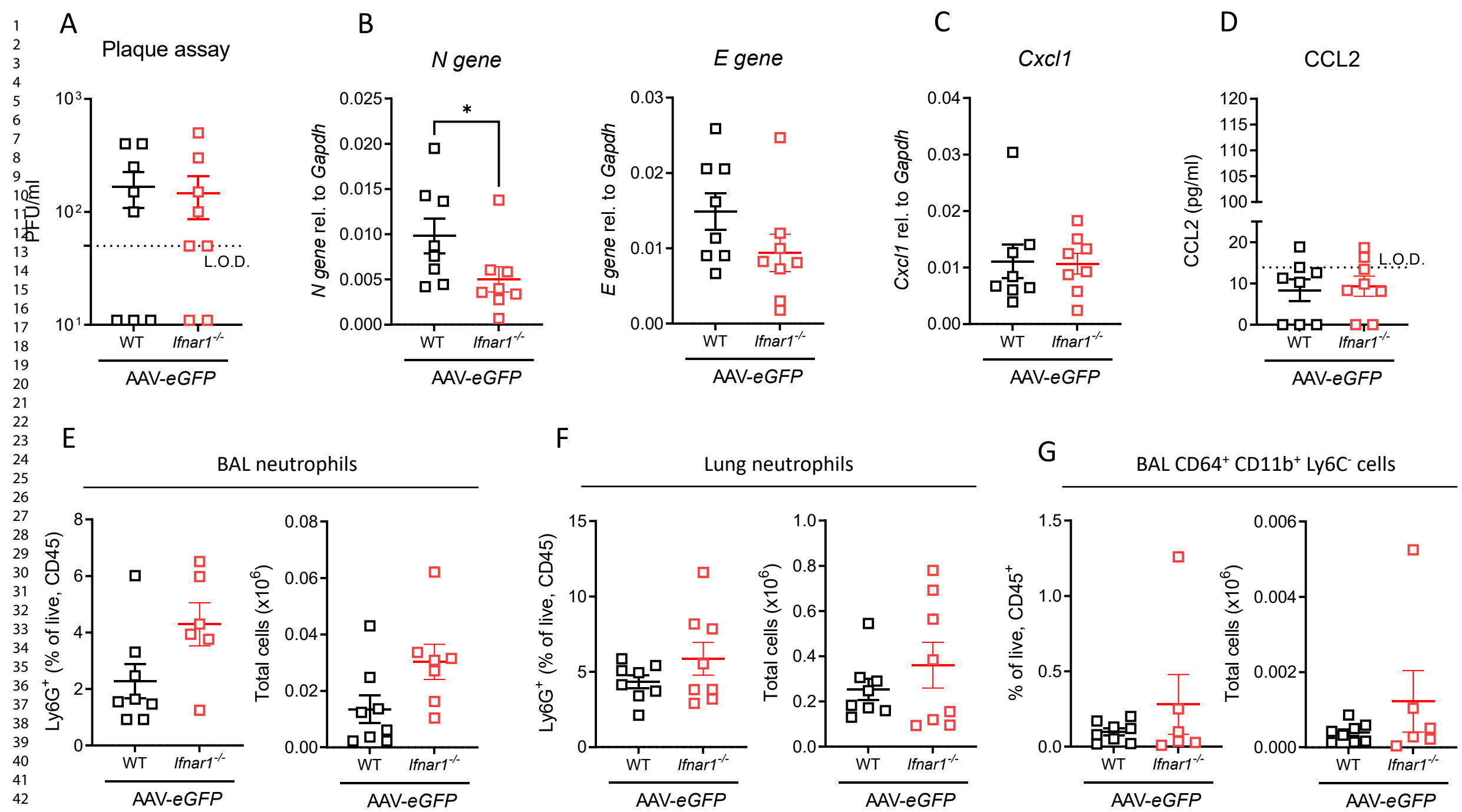
Fig3 eps format

154x124mm (300 x 300 DPI)



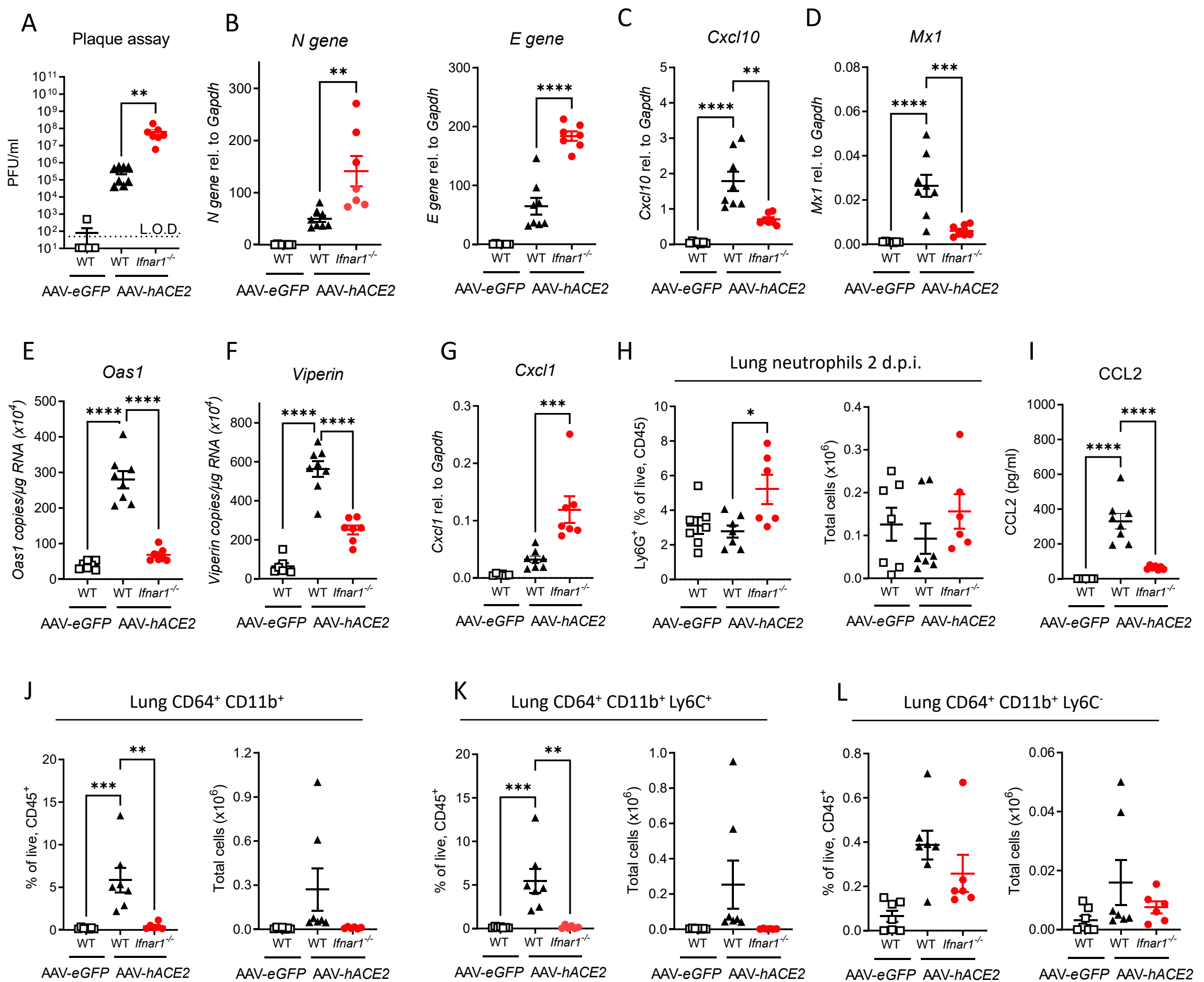
Supplemental Figure 1: Validation of *hACE2* transduction and interferon expression upon SARS-CoV-2 infection

A) *eGFP* signal in lung cryosections of WT or *Ifnar1*^{-/-} transduced with rAAV-*eGFP* (20 days post transduction), or vehicle (PBS). Representative images shown for each group (2-3 mice per group). Scale bar = 100 μ m. B) Expression of IFN- α and IFN- β in BAL fluid at 2 d.p.i. measured by Luminex Procarta assay. C) Expression of IFN- λ in BAL fluid at 2 d.p.i. measured by ELISA. Data are shown as mean \pm SEM. Two independent experiments per time point, data pooled, n = 6-8 per group. One Way ANOVA + Tukey's multiple comparison test; * indicates significant difference between WT rAAV-*hACE2* and *Ifnar1*^{-/-} rAAV-*hACE2*, * P < 0.05, ** P < 0.01, *** P < 0.005, **** P < 0.001.



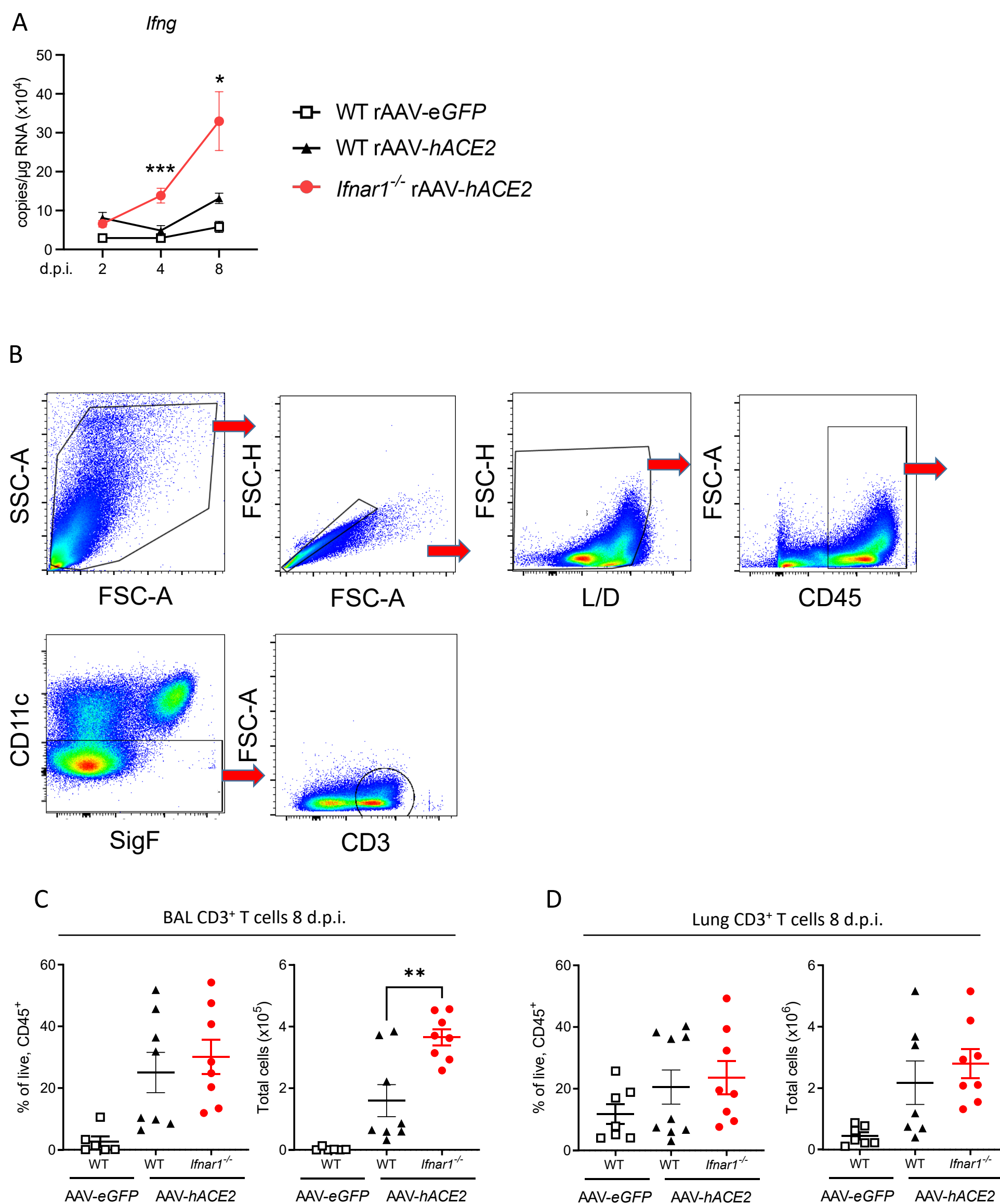
Supplemental Figure 2: Baseline viral load and immune response at 0.75 d.p.i. with SARS-CoV-2 in rAAV-eGFP transduced WT and *Ifnar1*^{-/-} mice

WT and *Ifnar1*^{-/-} mice were transduced with rAAV-eGFP and after 20 days infected with SARS-CoV-2 (D614G, 2x10⁶ PFU/mouse). BAL and lungs were analysed at 0.75 d.p.i. A) Viral load measured by plaque assay on Vero cells overexpressing *hACE2* and *TMPRESS2* B) Expression of SARS-CoV-2 *N gene* (nucleocapsid phosphoprotein) and *E gene* (envelope protein) in lung tissue relative to *Gapdh*, measured by RT-PCR C) Gene expression of *Cxcl1* in lung tissue relative to *Gapdh*. D) Protein expression of CCL2 in BAL fluid measured by ELISA. E-F) Proportions of live, CD45⁺ and total numbers of neutrophils in BAL (E) and lung (F) at 0.75 d.p.i. G) Proportions of live, CD45⁺ and total numbers of CD64⁺ CD11b⁺ Ly6C⁺ monocytes in BAL at 0.75 d.p.i. Data are shown as mean ± SEM. Two independent experiments, data pooled, n = 6-8 per group. One Way ANOVA + Tukey's multiple comparison test; * indicates significant difference between WT AAV-*hACE2* and *Ifnar1*^{-/-} AAV-*hACE2*, * P < 0.05.



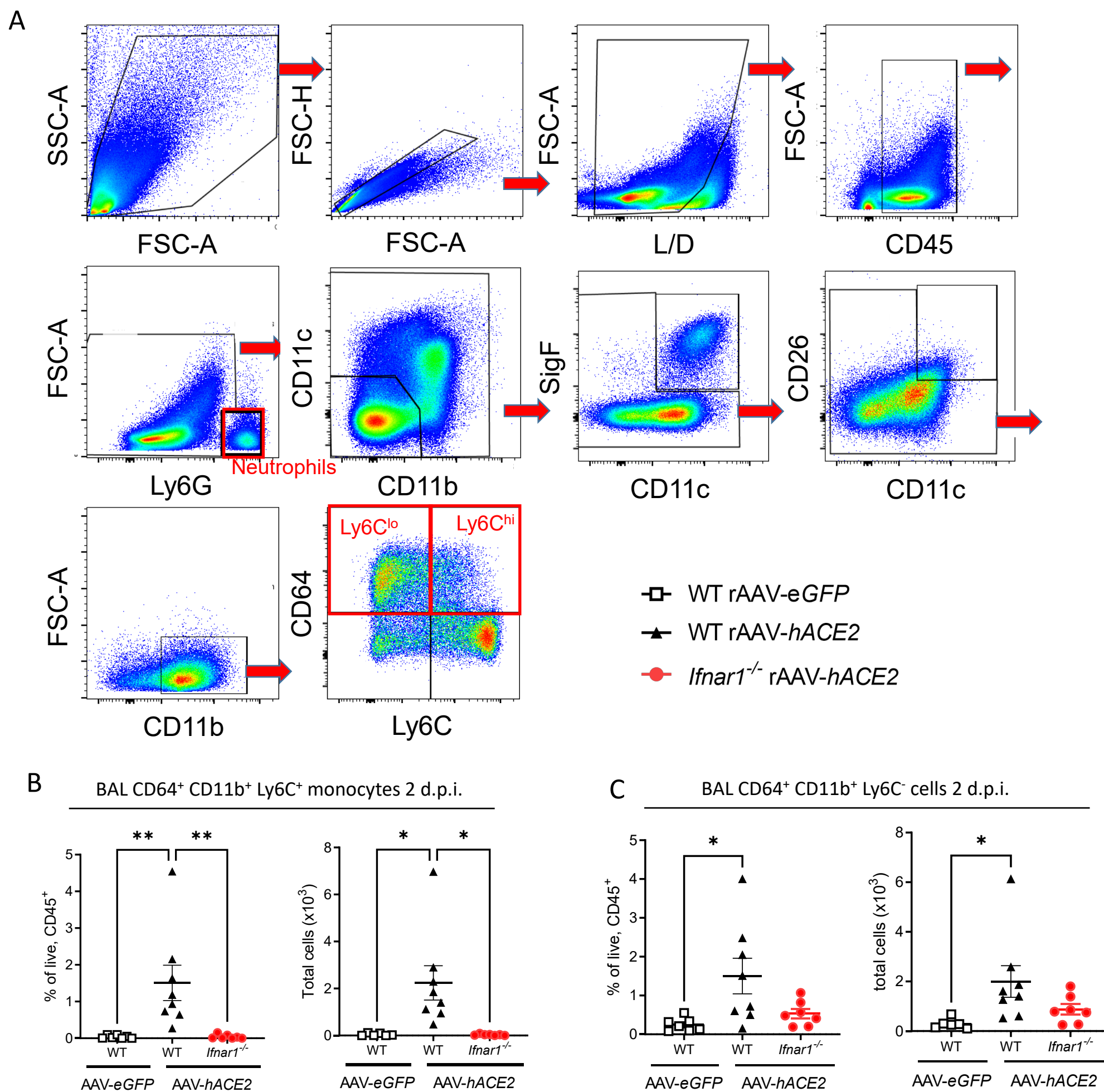
Supplemental Figure 3: Viral load and immune responses at 2 d.p.i. with SARS-CoV-2 in rAAV-hACE2 mouse model

WT and *Ifnar1*^{-/-} mice were transduced with rAAV-eGFP or rAAV-hACE2 and after 20 days infected with SARS-CoV-2 (D614G, 2x10⁶ PFU/mouse). BAL and lungs were analysed at 2 d.p.i. A) Viral load measured by plaque assay on Vero cells overexpressing hACE2 and TMPRESS2 B) Expression of SARS-CoV-2 *N gene* (nucleocapsid phosphoprotein) and *E gene* (envelope protein) in lung tissue relative to *Gapdh*, measured by RT-PCR C-F) Gene expression analysis of IFN stimulated genes (ISG) *Cxcl10* (C), *Mx1* (D), *Oas1* (E) and *Viperin* (F) measured by RT-PCR, relative to expression of *Gapdh* or total copy numbers normalized to expression of *Gapdh* (*Oas1* and *Viperin*). G) Gene expression of *Cxcl1* in lung tissue relative to *Gapdh*. H) Protein expression of CCL2 in BAL fluid measured by ELISA. I) Proportions of live, CD45⁺ and total numbers of neutrophils in lung tissue J - L) Proportions of live, CD45⁺ and total numbers of CD64⁺ CD11b⁺ inflammatory myeloid cells (J), CD64⁺CD11b⁺Ly6C⁺ cells (K) and CD64⁺CD11b⁺Ly6C⁻ cells (L) in lung tissue. Data are shown as mean ± SEM. Tissues were collected at 2 d.p.i. Two independent experiments per time point, data pooled, n = 6-8 per group. One Way ANOVA + Tukey's multiple comparison test; * indicates significant difference between WT AAV-hACE2 and *Ifnar1*^{-/-} AAV-hACE2, * P < 0.05, ** P < 0.01, *** P < 0.005, **** P < 0.001.



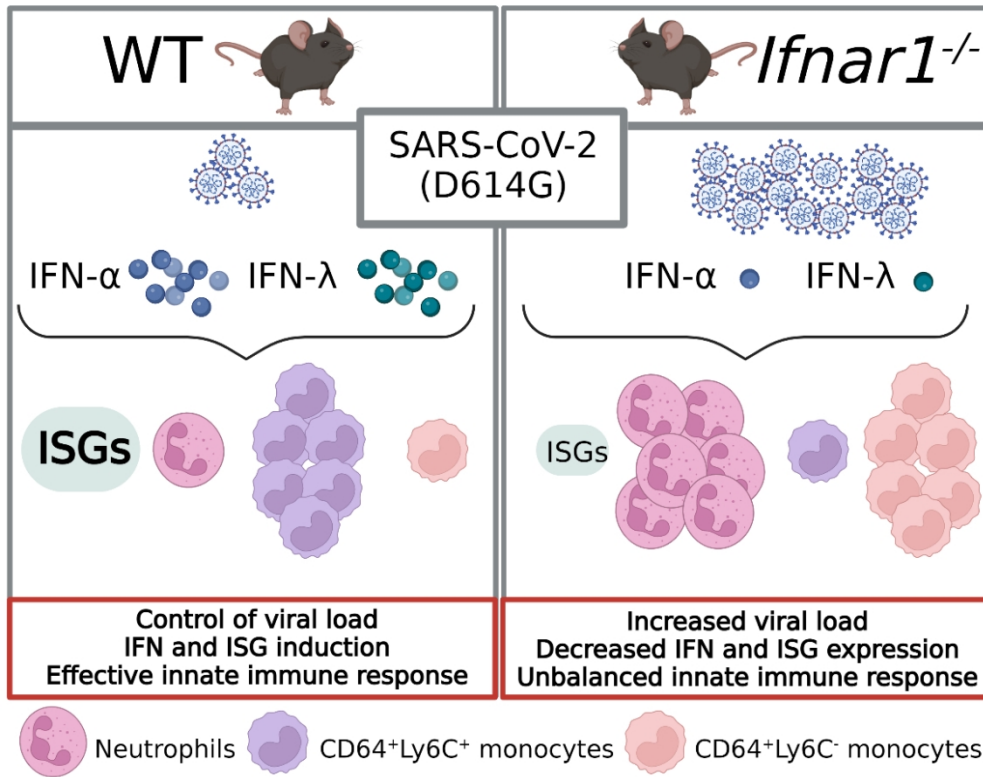
Supplemental Figure 4: Interferon- γ and T cell recruitment to the lungs upon infection SARS-CoV-2 in rAAV-*hACE2* mouse model

A) Gene expression analysis of *Ifng* measured in lung homogenates by RT-PCR, total copy numbers normalized to expression of *Gapdh* at 2, 4 and 8 days. B) Gating strategy to detect CD3⁺ T cells in BAL and lung 8 days after infection with SARS-CoV-2. C – D) Proportions of live, CD45⁺ and total numbers of T cells in BAL (C) and lung (D) at 8 d.p.i. Data are shown as mean \pm SEM. Two independent experiments per time point, data pooled, n = 6-8 per group. One Way ANOVA + Tukey's multiple comparison test per time point; * P < 0.05, ** P < 0.01, *** P < 0.005, **** P < 0.001.



Supplemental Figure 5: Myeloid cell recruitment into the airways upon infection SARS-CoV-2 in rAAV-hACE2 mouse model

A) Gating strategy to detect innate immune cell populations in BAL and lung after infection with SARS-CoV-2. Populations of interest (highlighted in red) are Ly6G⁺ neutrophils, CD11b⁺CD64⁺Ly6C⁻ and CD11b⁺CD64⁺Ly6C⁺ inflammatory myeloid cells. B-C) Proportions of live, CD45⁺ and total numbers of CD64⁺ CD11b⁺ Ly6C⁺ monocytes (C) and CD64⁺ CD11b⁺ Ly6C⁻ monocytes (D) in BAL at 2 d.p.i. Data are shown as mean ± SEM. Two independent experiments per time point, data pooled, n = 6-8 per group. One Way ANOVA + Tukey's multiple comparison test; * P < 0.05, ** P < 0.01, *** P < 0.005, **** P < 0.001.



127x101mm (236 x 236 DPI)

1
2
3 During SARS-CoV-2 infection in mice, IFNAR1-deficiency results in dysregulated innate immune
4 responses, such as increased neutrophil recruitment to the lung and an altered monocyte population
5 profile. Together with decreased expression of anti-viral effector interferon-stimulated genes *Mx1*,
6 *Oas1* and *Viperin* this results in higher viral loads and overall worsened disease phenotype.
7
8
9
10
11
12
13
14
15
16
17
18
19
20
21
22
23
24
25
26
27
28
29
30
31
32
33
34
35
36
37
38
39
40
41
42
43
44
45
46
47
48
49
50
51
52
53
54
55
56
57
58
59
60

For Peer Review